Iron pnictides as a new setting for quantum criticality

Jianhui Dai[a], Qimiao Si[b], Jian-Xin Zhu[c], and Elihu Abrahams[d,1]

[a]Zhejiang Institute of Modern Physics, Zhejiang University, Hangzhou 310027, China; [b]Department of Physics and Astronomy, Rice University, Houston, TX 77005; [c]Theoretical Division, Los Alamos National Laboratory, Los Alamos, NM 87545; and [d]Department of Physics and Astronomy, Center for Materials Theory, Rutgers University, Piscataway, NJ 08855

Contributed by Elihu Abrahams, January 26, 2009 (sent for review December 26, 2008)

Two major themes in the physics of condensed matter are quantum critical phenomena and unconventional superconductivity. These usually occur in the context of competing interactions in systems of strongly correlated electrons. All this interesting physics comes together in the behavior of the recently discovered iron pnictide compounds that have generated enormous interest because of their moderately high-temperature superconductivity. The ubiquity of antiferromagnetic ordering in their phase diagrams naturally raises the question of the relevance of magnetic quantum criticality, but the answer remains uncertain both theoretically and experimentally. Here, we show that the undoped iron pnictides feature a unique type of magnetic quantum critical point, which results from a competition between electronic localization and itinerancy. Our theory provides a mechanism to understand the experimentally observed variation of the ordered moment among the undoped iron pnictides. We suggest P substitution for As in the undoped iron pnictides as a means to access this example of magnetic quantum criticality in an unmasked fashion. Our findings point to the iron pnictides as a much-needed setting for quantum criticality, one that offers a unique set of control parameters.

magnetism | phase transition | electron correlation

The recent discovery of copper-free high-T_c superconductors has triggered intense interest in the homologous iron pnictides. The parent compound of the lanthanum-iron oxyarsenide, LaOFeAs (1), exhibits a tetragonal-orthorhombic structural transition and long-range antiferromagnetic order (2). Electron doping, via fluorine substitution for oxygen, suppresses both and induces superconductivity. Other families of the arsenide compounds show a similar interplay among structure, antiferromagnetism, and superconductivity. These include the oxyarsenide systems obtained through replacing lanthanum by other rare-earth elements such as Ce, Pr, Nd, Sm, and Gd (3–6), as well as oxygen-free arsenides, such as $BaFe_2As_2$ (7) and $SrFe_2As_2$ (8).

Quantum Criticality in the Pnictides

The existence of the antiferromagnetic state naturally raises the possibility of carrier-doping-induced quantum phase transitions in the iron pnictides (9–11), but the situation is not yet certain. Theoretically, the evolution of the Fermi surface as a function of carrier doping is not yet well understood, and this limits the study of quantum criticality. Experimentally, earlier measurements in $LaO_{1-x}F_xFeAs$ (1) and $SmO_{1-x}F_xFeAs$ (12) show a moderate suppression of the magnetic/structural transition temperature(s) as x is increased; beyond x of about $\sim$7%, the transitions are interrupted by superconductivity. Further experiments have led to conflicting reports for the first-order or second-order nature of the carrier-induced zero-temperature magnetic and structural phase transitions (13–15).

We propose that an alternative to a possible doping-induced quantum phase transition is one that is accessed by changing the relative strength of electron–electron correlations. Thus, we suggest that the iron pnictides may exhibit an example and setting for quantum criticality. Our approach is motivated by the phenomenological and theoretical evidence that the parent iron pnictide is a "bad metal" (9, 16, 17). Accordingly, we formulate our considerations in terms of an *incipient* Mott insulator: the electron–electron interactions lie close to, but do not exceed the critical value for the insulating state. Within this picture, the electronic excitations comprise an incoherent part away from the Fermi energy, and a coherent part in its vicinity. The incoherent electronic excitations are described in terms of localized Fe magnetic moments, with frustrating superexchange interactions. The latter have been discussed earlier by two of us (9) and others (18). This division of the electron spectrum is a simple and convenient way of analyzing the complex behavior of a bad metal close to the Mott transition, whose spectrum exhibits incipient upper and lower Hubbard bands and a coherent quasi-particle peak at the Fermi energy (19).

The coupling of the local moments to the coherent electronic excitations competes against the magnetic ordering. A magnetic quantum critical point arises when the spectral weight of the coherent electronic excitations is increased to some threshold value.

The Electron Spectrum

The incoherent and coherent parts of the single-electron spectral function are illustrated schematically in Fig. 1. The central peak describes the coherent itinerant carriers; these are the electronic excitations that are responsible for a Drude optical response and that are adiabatically connected to their noninteracting counterparts. The side peaks describe the incoherent excitations, vestiges of the lower and upper Hubbard bands associated with a Mott insulator that would arise if the electron–electron interactions were larger than the Mott localization threshold. Each of the three peaks may in general have a complex structure due to the multiorbital nature of the iron pnictides. The decomposition of the electronic spectral weight into coherent and incoherent parts is natural for a metal near a Mott transition (19, 20).

We use w to denote the percentage of the spectral weight lying in the coherent part of the spectrum. A relatively small w may be inferred for the iron pnictides, because the Drude weight seen in the optical conductivity (21–23) is very small (on the order of 5% of the total spectral weight integrated to $\approx$2 eV). A small w corresponds to an interaction strength sufficiently large that the system is close to the Mott transition, albeit on the metallic side; this implies a large electron–electron scattering rate, consistent with the observed large electrical resistivity (on the order of 0.5 m$\Omega \cdot$ cm for single crystals and 5 m$\Omega \cdot$ cm for polycrystals) at room temperature. In terms of electrical conduction, the iron pnictides are similar to, e.g., V_2O_3, a bad metal (with a room temperature resistivity (24) of about 0.5 m$\Omega \cdot$ cm) that is known to be on the verge of a Mott transition, and is very different from, e.g., Cr, a simple metal [with a room temperature resistivity (25) of $\approx$0.01 m$\Omega \cdot$ cm] which orders into a spin-density-wave ground state.

Author contributions: J.D., Q.S., J.-X.Z., and E.A. designed research; J.D., Q.S., J.-X.Z., and E.A. performed research; and Q.S. and E.A. wrote the paper.

The authors declare no conflict of interest.

[1]To whom correspondence should be addressed. E-mail: abrahams@physics.rutgers.edu.

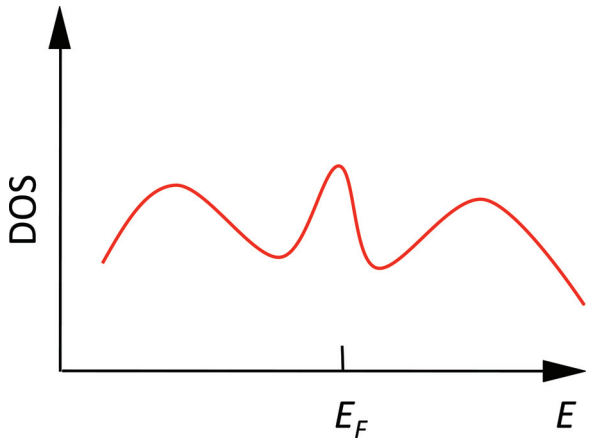

Fig. 1. Single-electron spectral function as the sum of coherent and incoherent parts. The single-electron density of states (DOS) is plotted against energy (E); E_F is the Fermi energy. Each peak may contain additional structure due to the multiorbital nature of the iron pnictides. The percentage of the total spectral weight that belongs to the coherent part is defined as w, which goes from 1 when the interaction is absent, to 0 when the interaction reaches and goes beyond the Mott-transition threshold.

Effective Hamiltonian

To study the magnetism, the incoherent spectrum is naturally described in terms of localized magnetic moments, leading to a matrix J_1–J_2 model (9):

$$H_J = \sum_{\langle ij\rangle} J_1^{\alpha\beta}\mathbf{s}_{i,\alpha}\cdot\mathbf{s}_{j,\beta} + \sum_{\langle\langle ij\rangle\rangle} J_2^{\alpha\beta}\mathbf{s}_{i,\alpha}\cdot\mathbf{s}_{j,\beta} + J_H\sum_{i,\alpha\neq\beta}\mathbf{s}_{i,\alpha}\cdot\mathbf{s}_{i,\beta}. \quad [1]$$

Here, J_1 and J_2 label the superexchange interactions between two nearest-neighbor (n.n., $\langle ij\rangle$) and next-nearest-neighbor (n.n.n., $\langle\langle ij\rangle\rangle$) Fe sites, respectively. Both are matrices in the orbital basis, α,β with these indices summed when repeated. J_H is the Hund's coupling.

Eq. **1** reflects the projection of the full interacting problem to the low-energy subspace when the system is a Mott insulator ($w = 0$) and the single-electron excitations have only the incoherent part. When the single-electron excitations also contain the coherent part (w being nonzero but small, see Fig. 1), these coherent electronic excitations must be included in the low-energy subspace as well.

We will use the projection procedure of ref. 26 to construct the effective low-energy Hamiltonian. We denote by $d^{\rm coh}_{\mathbf{k}\alpha\sigma}$ the d-electron operator projected to the coherent part of the electronic states near the Fermi energy, and define the incoherent part through $d_{\mathbf{k}\alpha\sigma}\equiv d^{\rm coh}_{\mathbf{k}\alpha\sigma}+d^{\rm incoh}_{\mathbf{k}\alpha\sigma}$. Therefore, unlike the full d-electron operator, $d^{\rm coh}_{\mathbf{k}\alpha\sigma}$ does not satisfy the fermion anticommutation rule. Indeed, its spectral function integrated over frequency defines w. We therefore introduce $c_{\mathbf{k}\alpha\sigma} = (1/\sqrt{w})d^{\rm coh}_{\mathbf{k}\alpha\sigma}$, so that $c_{\mathbf{k}\alpha\sigma}$ has a total spectral weight of 1 and satisfies $\{c_{\mathbf{k}\alpha\sigma}, c^\dagger_{\mathbf{k}\alpha\sigma}\} = 1$.

We then have the effective low-energy Hamiltonian terms for the coherent itinerant carriers (H_c) and for their mixing with the local moments (H_m):

$$H_c = \sum_{\mathbf{k},\alpha,\sigma}\epsilon_{\mathbf{k}\alpha\sigma}c^\dagger_{\mathbf{k}\alpha\sigma}c_{\mathbf{k}\alpha\sigma} = w\sum_{\mathbf{k},\alpha,\sigma}E_{\mathbf{k}\alpha\sigma}c^\dagger_{\mathbf{k}\alpha\sigma}c_{\mathbf{k}\alpha\sigma}$$

$$H_m = \sum_{\mathbf{kq}\alpha\beta\gamma} g_{\mathbf{k},\mathbf{q}\alpha\beta\gamma}c^\dagger_{\mathbf{k}+\mathbf{q}\alpha\sigma}\frac{\boldsymbol{\tau}_{\sigma\sigma'}}{2}c_{\mathbf{k}\beta\sigma'}\cdot\mathbf{s}_{\mathbf{q}\gamma} = w\sum_{\mathbf{kq}\alpha\beta\gamma} G_{\mathbf{k},\mathbf{q}\alpha\beta\gamma}c^\dagger_{\mathbf{k}+\mathbf{q}\alpha\sigma}\frac{\boldsymbol{\tau}_{\sigma\sigma'}}{2}c_{\mathbf{k}\beta\sigma'}\cdot\mathbf{s}_{\mathbf{q}\gamma}. \quad [2]$$

Here, $\boldsymbol{\tau}$ labels the three Pauli matrices. In the projection procedure leading to Eq. **2**, we keep $d^{\rm coh}_{\mathbf{k}\alpha\sigma}$ as part of the low-energy degrees of freedom; the prefactor w in the first equation comes from the rescaling $c_{\mathbf{k}\alpha\sigma} = (1/\sqrt{w})d^{\rm coh}_{\mathbf{k}\alpha\sigma}$ and $E_{\mathbf{k}\alpha\sigma}$ is therefore the conduction–electron dispersion at $w = 1$. At the same time, we integrate out the high-energy states involved in $d^{\rm incoh}_{\mathbf{k}\alpha\sigma}$. To the leading order in w, this procedure is carried out at the $w = 0$ point which is taken to have a full gap (26); as a result, the effective coupling $G_{\mathbf{kq}\alpha\beta\gamma}$ is of order w^0. Beyond the leading order in w, the coupling constants will acquire further corrections. The computation of these corrections is difficult, since, at those orders, the spectrum becomes continuous from the coherent to incoherent part (Fig. 1); it is left for future work. Still, our leading-order analysis captures the form of the low-energy effective Hamiltonian, which is

$$H_{eff} = H_J + H_c + H_m. \quad [3]$$

J_1–J_2 Competition

The superexchange interactions in the iron pnictides contain n.n. and n.n.n. terms because of the specific relative locations of the ligand As atoms and Fe atoms (9, 18, 27). To assess the tunability of J_1 and J_2, we consider an oversimplified case, illustrated in Fig. 2. Here, only one Fe 3d orbital is considered. We assume that the 3d orbital on each of the 4 corners of a square plaquette has an identical hybridization matrix element, V, with one As 4p orbital located above the center of the plaquette. The superexchange interaction is found to be $h_J \propto \sum_{\mathbf{r}}[\sum_\square \mathbf{s}(\mathbf{r})]^2$, where $\mathbf{r}$ labels a plaquette in the 2D square lattice and the summation $\sum_\square$ is over the 4 Fe sites of a plaquette. For classical spins, this is the canonical case of magnetic frustration: all states with $\sum_\square \mathbf{s}(\mathbf{r}) = 0$ are degenerate. Written in the form of Eq. **1**, this corresponds to $J_2 = J_1/2$. This discussion is instructive for the understanding of the realistic exchange interactions in the iron pnictides. Several aspects are neglected in the simplified analysis given above. First, multiple 3d orbitals are important, and the hybridization is orbital-sensitive. Both the J_1 and J_2 interactions are therefore matrices. Second, the real band structures must be described by more complex d-p, p-p, and d-d tight-binding parameters. Both features spoil the elementary $J_2 = J_1/2$ relationship. Still, the simple considerations given above suggest that the overall strength of J_2 and J_1, i.e., the largest eigenvalues of the J_2 and J_1 matrices, are comparable with each other. Detailed analysis of the matrix elements indicates that there are more entries in the J_2 matrix than in the J_1 matrix that correspond to the dominating antiferromagnetic component, and that the overall magnitude (the largest eigenvalue) of the J_2 matrix will be somewhat larger than half of that of the J_1 matrix. This conclusion is supported by the fitting of the ab initio results

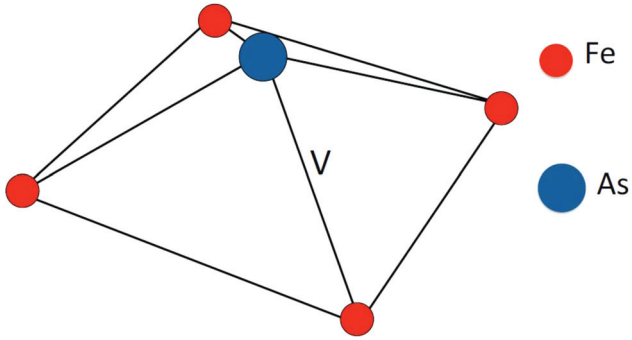

Fig. 2. A square plaquette of Fe ions, with an As ion sitting above or below the center of the plaquette. The hybridization term is written as $h_V = \sum_{\boldsymbol{r}} V[p^\dagger_\sigma(\boldsymbol{r})\sum_\square d_\sigma(\boldsymbol{r}) + h.c.]$, and the energy levels for the Fe 3d orbital and As 4p orbital are ϵ_d and ϵ_p, respectively. The resulting superexchange interaction is $h_J = [2V^4/(\epsilon_p-\epsilon_d)^3]\sum_{\boldsymbol{r}}[\sum_\square \boldsymbol{s}(\boldsymbol{r})]^2$.

PHYSICS

of the ground-state energies for various magnetic configurations in terms of J_1 and J_2 parameters in the (nonmatrix) Heisenberg form (18, 27). This range of J_2/J_1 leads to a two-sublattice collinear antiferromagnetic ground state, consistent with the results of the neutron scattering experiment (2).

On the one hand, the above argument implies that the magnetic frustration effect is strong, and can provide significant quantum fluctuations leading to a reduced ordered moment. On the other hand, it suggests that the degree to which J_2/J_1 can be tuned in practice could be limited.

Magnetic Quantum Critical Point

The order parameter for the two-sublattice antiferromagnet appropriate for $J_2/J_1 > 1/2$ is the staggered magnetization, $\mathbf{m}$, at wave vector $\mathbf{Q} = (\pi, 0)$. The effective theory for the H_J term alone corresponds to a ϕ^4 theory whose action is of the form $\mathcal{S} \sim r\phi^2 + u\phi^4$. The coupling to the coherent quasi-particles is given by the H_m term of Eq. **2**; it causes a shift of the tuning parameter r and also introduces a damping term. These contributions to the r coefficient are given by:

$$\Delta r + i\Gamma = \sum_{\mathbf{k},\alpha,\beta,\gamma} g^2_{\mathbf{kq}\alpha\beta\gamma} a^2_\gamma \frac{f(\epsilon_{\mathbf{k}+\mathbf{q},\alpha}) - f(\epsilon_{\mathbf{k},\beta})}{i\omega_n - (\epsilon_{\mathbf{k}+\mathbf{q},\alpha} - \epsilon_{\mathbf{k},\beta})}. \qquad [4]$$

Here, $f(\epsilon)$ is the Fermi–Dirac distribution function and a_γ is an orbital-dependent coefficient: $\sum_\gamma a_\gamma \mathbf{s}_\gamma$ appears in the order parameter for the $(\pi, 0)$ antiferromagnet. Note that both $g_{\mathbf{k},\mathbf{q}\alpha\beta\gamma}$ and $\epsilon_{\mathbf{k},\beta}, \epsilon_{\mathbf{k}+\mathbf{q},\alpha}$ are linear order in w. We can infer from Eq. **4** that the damping term is of the order w^0 at low energies: for $|\omega_n| \ll wW$ (W is the bandwidth), $\Gamma = \gamma|\omega_n|$, where γ is, to leading order in w, the constant value associated with the couplings and density of states of the $w = 1$ case. Note that γ is nonzero because, for the parent compounds, $\mathbf{Q}$ connects the hole pockets near the Γ point of the Brillouin zone (BZ) and the electron pockets near the M points (in the unfolded BZ notation). At the same time, γ does not diverge since the nesting is not perfect. The existence of the linear in ω damping term is in contrast to the doped case, where $\mathbf{Q}$ no longer connects the hole- and electron-Fermi surfaces (11). Importantly, we can also infer from Eq. **4** that the leading frequency- and temperature-independent term $\Delta r = wA_\mathbf{Q}$ is linear in w, with $A_\mathbf{Q} = \sum_{\mathbf{k},\alpha,\beta,\gamma} G^2_{\mathbf{kq}\alpha\beta\gamma} a^2_\gamma [\Theta(E_F - E_{\mathbf{k}+\mathbf{Q}}) - \Theta(E_F - E_\mathbf{k})]/(E_{\mathbf{k},\beta} - E_{\mathbf{k}+\mathbf{Q},\alpha})$ (where Θ is the Heaviside function) is independent of w, and positive.

The low-energy Ginzburg–Landau theory then takes the form,

$$\mathcal{S} = \int d\mathbf{q} \int d\omega [r(w) + c(\mathbf{q} - \mathbf{Q})^2 + \omega^2 + \gamma|\omega|][\mathbf{m}(\mathbf{q}, \omega)]^2 + u \prod_{i=1}^{4} \int d\mathbf{q}_i \int d\omega_i \, \delta\left(\sum_i \mathbf{q}_i\right) \delta\left(\sum_i \omega_i\right) [\mathbf{m}]^4 + \ldots, \qquad [5]$$

where $r(w) = r(w = 0) + wA_\mathbf{Q}$. $r(w = 0)$ is negative, placing the system at $w = 0$ to be antiferromagnetically ordered. The linear in w shift, $wA_\mathbf{Q}$, causes $r(w)$ to vanish at a $w = w_c$, leading to a quantum critical point. In terms of the external control parameter δ, shown in Fig. 3, $w = w_c$ defines $\delta = \delta_c$. The ϕ^4 theory describes a $z = 2$ (where z is the dynamical exponent) antiferromagnetic quantum phase transition, which is generically second order.

The $O(3)$ vector $\mathbf{m}$, corresponding to the $(\pi, 0)$ order, is accompanied by another $O(3)$ vector, $\mathbf{m}'$ that describes the $(0, \pi)$ order. These two vector order parameters accommodate a composite scalar, $\mathbf{m} \cdot \mathbf{m}'$, the order parameter for an Ising transition (10, 11, 28). In turn, the Ginzburg–Landau action, Eq. **5**, contains a quartic coupling $\tilde{u}(\mathbf{m} \cdot \mathbf{m}')^2$ [as well as $u'\mathbf{m}^2(\mathbf{m}')^2$]. In the $z = 2$ case here, the ϕ^4 theory is at effective dimension $d + z = 4$. At the QCP of the $O(3)$ transition, the $\tilde{u}$ quartic coupling term is marginally relevant in the renormalization group sense. The $T = 0$ transition could therefore either be turned to first order, or be split into two continuous transitions, one for the Ising transition, whose scalar order parameter is $\vec{m} \cdot \vec{m}'$ (which corresponds to the structural distortion when it is coupled to some structural degrees of freedom), the other is for the $O(3)$ magnetic one. Either effect is expected to be weak, because of the marginal nature of the coupling.

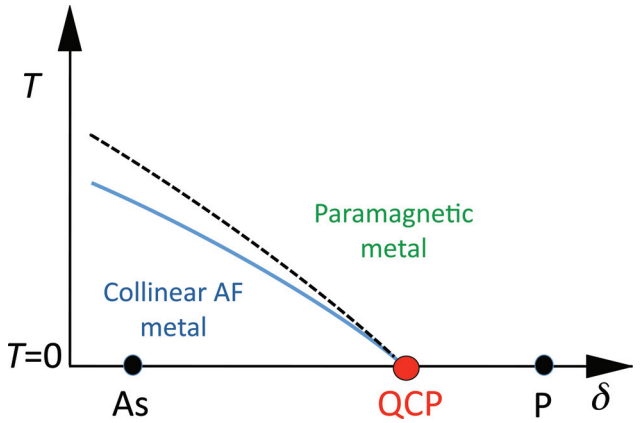

Fig. 3. Magnetic quantum phase transition in the parent compounds of the iron pnictides. The blue solid/black dashed lines represent the magnetic/structural transitions, respectively. δ is a nonthermal control parameter: increasing δ enhances the spectral weight in the coherent part of the single-electron excitations (Fig. 1). The QCP, at $\delta = \delta_c$, separates a two-sublattice collinear AF ground state from a paramagnetic one. A specific example for δ is the concentration of P doping for As: a parent iron pnictide with As is an antiferromagnetic metal, whereas its counterpart with P is nonmagnetic; the possibility that the latter is superconducting is not shown in the phase diagram.

The magnetic quantum criticality will strongly contribute to the electronic and magnetic properties in the quantum critical regime. We note that since $d = z = 2$, there are (marginal) logarithmic corrections to simple Gaussian critical behavior (29). Following discussions in, e.g., ref. 29, we expect that the specific-heat coefficient will be $C/T \sim \ln(1/T)$, the NMR relaxation rate $1/T_1 \propto$ const, and (in the presence of disorder scattering that smears the Fermi surface) the resistivity $\rho \propto T$.

Tuning Parameter and Variation of Magnetic Order

The parent materials of the different iron arsenides will have different internal pressures and "c/a" ratios, and will correspondingly have different ratios of the electron–electron interaction to the effective bandwidth. According to our theory, the resulting variation of the coherent spectral weight w will, in turn, tune the control parameter r in Eq. **5**, and the ordered moment will change accordingly across the different compounds.

Neutron scattering experiments have indeed found that the ordered moment does vary across the parent arsenides. The moment associated with Fe-ordering at low temperatures is ≈0.2-0.3 μ_B/Fe in NdOFeAs (30, 31), 0.4 μ_B/Fe in LaOFeAs (2), 0.5 μ_B/Fe in PrOFeAs (32, 33), and 0.8-1.0 μ_B/Fe in CeOFeAs (15), $BaFe_2As_2$ (34), and $SrFe_2As_2$ (35).

$As_{1-\delta}P_\delta$ Series of the Parent Iron Pnictides

Because the c-lattice constant in LaOFeP is smaller than that in LaOFeAs, these considerations suggest that the coherent-electron spectral weight of the iron phosphides is larger than that of the iron arsenides. A consequence is that, in contrast to the arsenide, the phosphide does *not* have a magnetic transition (36). We then propose that a parent iron pnictide series created by P doping of As presents a means to unmask a magnetic quantum critical point. Our purpose is better served the weaker the superconductivity is in the P end material. $LaOFeAs_{1-\delta}P_\delta$ is promising, since LaOFeP is a weak superconductor whose T_c is only a few Kelvin or may

even vanish (37–39). $CeOFeAs_{1-\delta}P_{\delta}$ may also be of interest in this context. While CeOFeAs (15) is antiferromagnetic, CeOFeP is a paramagnetic metal (40). We remark in passing that P-doping for As is more advantageous than external pressure, because the latter is known to cause a volume collapse (41). It would be interesting to search for a substitution for As such that w could be reduced, leading toward to the Mott insulating state.

To understand the tuning of the microscopic electronic parameters, we have carried out density-functional-theory (DFT) calculations on both CeOFeAs and CeOFeP for comparison. We find that the d-p hybridization matrix is larger in CeOFeP than in CeOFeAs. This is consistent with the qualitative consideration that, compared with CeOFeAs, CeOFeP has a higher internal pressure and, hence, a higher kinetic energy and smaller ratio of the interaction to the bandwidth, thus a larger coherent weight w.

Comparison with DFT Studies

We have considered the mechanism for quantum fluctuations having in mind the proximity to the Mott limit, where the *instantaneous* atomic moment is large (a few μ_B/Fe) to begin with. Most DFT calculations have shown that the *ordered* moment in the antiferromagnetic ground state is large, of the order 2 μ_B/Fe. Moreover, such a large ordered moment was found within DFT not only for the parent iron pnictides, but also for their doped counterparts.

Since DFT calculations neglect quantum fluctuations, we are tempted to interpret the large DFT-calculated moment as essentially the instantaneous atomic moment. Quantum fluctuations will then lead to a reduced ordered moment in the true ground state. The J_1–J_2 competition together with the coupling of the local moments to the coherent itinerant electronic excitations arising naturally in the Mott-proximity picture we have described is just such a mechanism for quantum fluctuations.

Discussion

We have developed a framework to describe the quantum magnetism of the iron pnictides, appropriate for electron–electron interactions that are of an intermediate strength to place the materials at the delicate boundary between itinerancy and localization. Our description takes into account the interplay between the itinerant and local-moment aspects, which are naturally associated with the interaction-induced coherent and incoherent parts of the electronic excitations. Enhancement of the spectral weight associated with the coherent electronic excitations weakens the magnetic order, and induces a magnetic quantum critical point. Our characterization of the magnetic excitations is important not only for the understanding of the existing and future experiments in the normal state, but also for the microscopic understanding of high-temperature superconductivity in the iron pnictides and related metallic systems close to a Mott transition. In addition, realization of a magnetic quantum critical point in the iron pnictides provides a new setting to explore some of the rich complexities (42, 43) of quantum criticality; this is much needed since quantum critical points have so far been explicitly observed only in a very small number of materials.

ACKNOWLEDGMENTS. We thank G. Cao, P. Coleman, C. Geibel, A. Jesche, C. Krellner, Z.-Y. Lu, E. Morosan, D. Natelson, C. Xu, and Z.A. Xu for useful discussions. This work was supported by the National Science Foundation of China, the 973 Program, and the Program for Changjian Scholars and Innovative Research Team in University (RT-0754) of the Education Ministry of China (J.D.), the Robert A. Welch Foundation (Q.S.), and the Department of Energy (J.-X.Z.).

1. Kamihara Y, Watanabe T, Hirano M, Hosono H (2008) Iron-based layered superconductor La[$O_{1-x}F_x$]FeAs ($x = 0.05 - 0.12$) with $T_c = 26$ K. *J Am Chem Soc* 130:3296–3297.
2. de la Cruz C, et al. (2008) Magnetic order close to superconductivity in the iron-based layered $LaO_{1-x}F_x$FeAs systems. *Nature* 453:899–902.
3. Chen GF, et al. (2008) Superconductivity at 41 K and its competition with spin-density-wave instability in layered $CeO_{1-x}F_x$FeAs. *Phys Rev Lett* 100:247002.
4. Ren ZA, et al. (2008) Superconductivity in the iron-based F-doped layered quaternary compound Nd[$O_{1-x}F_x$]FeAs. *Europhys Lett* 82:57002.
5. Chen XH, et al. (2008) Superconductivity at 43 K in $SmFeAsO_{1-x}F_x$. *Nature* 453:761–762.
6. Wang C, et al. (2008) Thorium-doping induced superconductivity up to 56 K in $Gd_{1-x}Th_x$FeAsO. *Europhys Lett* 83:67006.
7. Rotter M, et al. (2008) Spin-density-wave anomaly at 140 K in the ternary iron arsenide $BaFe_2As_2$. *Phys Rev B* 78:020503(R).
8. Krellner C, et al. (2008) Magnetic and structural transitions in layered iron arsenide systems: AFe_2As_2 versus RFeAsO. *Phys Rev B* 78:100504(R).
9. Si Q, Abrahams E (2008) Strong correlations and magnetic frustration in the high T_c iron pnictides. *Phys Rev Lett* 101:076401.
10. Fang C, Yao H, Tsai W-F, Hu J, Kivelson S (2008) A theory of electron nematic order in LaFeAsO. *Phys Rev B* 77:224509.
11. Xu C, Mueller M, Sachdev, S (2008) Ising and spin orders in the iron-based superconductors. *Phys. Rev. B* 78:020501(R).
12. Liu RH, et al. (2008) Anomalous transport properties and phase diagram of the FeAs-based $SmFeAsO_{1-x}F_x$ superconductors. *Phys Rev Lett* 101:087001.
13. Luetkens H, et al. (2008) Electronic phase diagram of the $LaO_{1-x}F_x$FeAs superconductor. arXiv:0806.3533v1 [cond-mat.supr-con].
14. Drew AJ, et al. (2008) Coexistence of static magnetism and superconductivity in $SmFeAsO_{1-x}F_x$ as revealed by muon spin rotation. arXiv:0807.4876v2 [cond-mat.supr-con].
15. Zhao J, et al. (2008) Structural and magnetic phase diagram of $CeFeAsO_{1-x}F_x$ and its relation to high-temperature superconductivity. *Nat Mater* 7:953–959.
16. Haule K, Shim JH, Kotliar G (2008) Correlated electronic structure of $LaO_{1-x}F_x$FeAs. *Phys Rev Lett* 100:226402.
17. Laad MS, Craco L, Leoni S, Rosner H (2008) Mottness underpins the anomalous optical response of iron pnictides. arXiv:0810.1607v1 [cond-mat.supr-con].
18. Yildirim T (2008) Origin of the 150-K Anomaly in LaFeAsO: Competing antiferromagnetic interactions, frustration, and a structural phase transition. *Phys Rev Lett* 101:057010.
19. Georges A, Kotliar G, Krauth W, Rozenberg MJ (1996) Dynamical mean-field theory of strongly correlated fermion systems and the limit of infinite dimensions. *Rev Mod Phys* 68:13–125.
20. Mo S-K, et al. (2006) Photoemission study of $(V_{1-x}M_x)_2O_3$ (M=Cr,Ti). *Phys Rev B* 74:165101.
21. Dong J, et al. (2008) Competing orders and spin-density-wave instability in La($O_{1-x}F_x$)FeAs. *Europhys Lett* 83:27006.
22. Boris AV, et al. (2008) Signatures of electronic correlations in optical properties of $LaFeAsO_{1-x}F_x$. arXiv:0806.1732v3 [cond-mat.supr-con].
23. Hu WZ, et al. (2008) Origin of the spin density wave instability in AFe_2As_2 (A=Ba, Sr) as revealed by optical spectroscopy. arXiv:0806.2652v4 [cond-mat.supr-con].
24. McWhan DB, et al. (1971) Electronic specific heat of metallic Ti-Doped V_2O_3. *Phys Rev Lett* 27:941–943.
25. Yeh A, et al. (2002) Quantum phase transition in a common metal. *Nature* 419: 459–462.
26. Moeller G, Si Q, Kotliar G, Rozenberg M, Fisher DS (1995) Critical behavior near the Mott transition in the Hubbard model. *Phys Rev Lett* 74:2082–2085.
27. Ma F, Lu Z-Y, Xiang T (2008) Antiferromagnetic superexchange interactions in LaOFeAs. arXiv:0804.3370v3 [cond-mat.supr-con].
28. Chandra P, Coleman P, Larkin AI (1990) Ising transition in frustrated Heisenberg models. *Phys Rev Lett* 64:88–91.
29. Löhneysen H, Rosch A, Vojta M, Wölfle P (2007) Fermi liquid instabilities at magnetic quantum phase transitions. *Rev Mod Phys* 79:1015–1075.
30. Qiu Y, et al. (2008) Structure and magnetic order in the NdFeAs(O,F) superconductor system. arXiv:0806.2195v2 [cond-mat.supr-con].
31. Chen Y, et al. (2008) Magnetic order of the iron spins in NdFeAsO. *Phys Rev B* 78: 064515.
32. Kimber SA, et al. (2008) Magnetic ordering and negative thermal expansion in PrFeAsO. arXiv:0807.4441v1 [cond-mat.supr-con].
33. Zhao J, et al. (2008) Lattice and magnetic structures of PrFeAsO, $PrFeAsO_{0.85}F_{0.15}$, and $PrFeAsO_{0.85}$. *Phys Rev B* 78:132504.
34. Huang Q, et al. (2008) Magnetic order in $BaFe_2As_2$, the parent compound of the FeAs based superconductors in a new structural family. arXiv:0806.2776v2 [cond-mat.supr-con].
35. Jesche A, et al. (2008) Strong coupling between magnetic and structural order parameters in $SrFe_2As_2$. arXiv:0807.0632v1 [cond-mat.supr-con].
36. Kamihara Y, et al. (2008) Electromagnetic properties and electronic structure of iron-based layered superconductor LaOFeP. *Phys Rev B* 77:214515.
37. Kamihara Y, et al. (2006) Iron-Based Layered Superconductor: LaOFeP. *J Am Chem Soc* 128:10012–10013.
38. Hamlin JJ, et al. (2008) Superconductivity in single crystals of LaFePO. *J Phys Condens Matter* 20:365220.
39. McQueen TM, et al. (2008) Intrinsic properties of stoichiometric LaFePO. *Phys Rev B* 78:024521.
40. Brüning EM, et al. (2008) CeFePO: A heavy fermion metal with ferromagnetic correlations. *Phys Rev Lett* 101:117206.
41. Kreyssig A, et al. (2008) Pressure-induced volume-collapsed tetragonal phase of $CaFe_2As_2$ as seen via neutron scattering. *Phys Rev B* 78:184517.
42. Sachdev S (2008) Quantum magnetism and criticality. *Nat Phys* 4: 173–185.
43. Gegenwart P, Si Q, Steglich F (2008) Quantum criticality in heavy-fermion metals. *Nat Phys* 4:186–197.